Pacific Northwest
NATIONAL LABORATORY

PNNL-38928

AA 7075 Sheet with 700 MPa Strength for Automotive Structural Components (CRADA 520) Final Report

December 2025

Amrita Lall
Katherine Rader
Sridhar Niverty
Vis Madhavan
Aashish Rohatgi

U.S. DEPARTMENT OF ENERGY

Prepared for the U.S. Department of Energy
under Contract DE-AC05-76RL01830

DISCLAIMER

PACIFIC NORTHWEST NATIONAL LABORATORY
operated by
BATTELLE
for the
UNITED STATES DEPARTMENT OF ENERGY
under Contract DE-AC05-76RL01830

Printed in the United States of America

Available to DOE and DOE contractors from the Office of Scientific and Technical Information,
P.O. Box 62, Oak Ridge, TN 37831-0062
www.osti.gov
ph: (865) 576-8401
fax: (865) 576-5728
email: reports@osti.gov

Available to the public from the National Technical Information Service
5301 Shawnee Rd., Alexandria, VA 22312
ph: (800) 553-NTIS (6847)
or (703) 605-6000
email: info@ntis.gov
Online ordering: http://www.ntis.gov

PNNL-38928

AA 7075 Sheet with 700 MPa Strength for Automotive Structural Components (CRADA 520) Final Report

December 2025

Amrita Lall
Katherine Rader
Sridhar Niverty
Vis Madhavan
Aashish Rohatgi

Prepared for
the U.S. Department of Energy
under Contract DE-AC05-76RL01830

Pacific Northwest National Laboratory
Richland, Washington 99354

Cooperative Research and Development Agreement (CRADA) Final Report

Report Date: December 2025

In accordance with Requirements set forth in the terms of the CRADA, this document is the CRADA Final Report, including a list of Subject Inventions, to be provided to PNNL Information Release who will forward to the DOE Office of Scientific and Technical Information as part of the commitment to the public to demonstrate results of federally funded research.

Parties to the Agreement: Fairmount Technologies, LLC and Pacific Northwest National Laboratory

CRADA number: 520

CRADA Title: AA 7075 Sheet with 700 MPa Strength for Automotive Structural Components

Responsible Technical Contact at DOE Lab: Aashish Rohatgi

Name and Email Address of POC at Company: Vis Madhavan, vis@fairmounttech.com

DOE Program Office: Vehicle Technology Office

Joint Work Statement Funding Table showing DOE funding commitment:

Funding	Project Year 1	Project Year 2	TOTALS
Government			
DOE	$125,000	$125,000	$250,000
Other			
Total Govt.	**$125,000**	**$125,000**	**$250,000**
Participant			
In-Kind	$200,000	$50,000	$250,000
Funds-In			
FAC			
Total Participant	**$200,000**	**$50,000**	**$250,000**
TOTAL CRADA Value	**$325,000**	**$175,000**	**$500,000**

Acknowledgments

The authors gratefully acknowledge support from the LightMAT Program within the Vehicles Technology Office, U.S. Department of Energy. The authors would like to acknowledge the support from following PNNL staff: Mark Rhodes, Ethan Nickerson, Timothy Roosendaal, and Rob Seffens in the mechanical test lab, and Irving Brown, Nate Brown, and Michael Blazon in the metallography lab. Finally, support by Fairmount Technologies personnel – Jordan Peter, Rajeshkumar Anandakumar, Jacob Chittum, Levi Helten, and Ross Frame is gratefully acknowledged.

Executive Summary

Fairmount Technologies (FT) is exploring a secondary benefit of their stretch roll forming process to produce ultra-high strength aluminum alloy AA 7075 sheets for potential automotive structural applications. Such sheets are expected to possess a nanocrystalline microstructure through cryo-rolling. And through their nano-structure derived high strength, these rolled sheets are expected to be an attractive feedstock for stamping high-strength, light-weight automotive components. Therefore, the goal of this project was to help FT develop their process, optimize the parameters to produce high-strength nanocrystalline AA 7075 sheets, and to characterize and optimize the strength and formability of the sheet produced. The target strength of the sheet was 700 MPa that is ~20% greater than the currently available AA7075 in its peak-aged T6 temper.

FT scaled up their third-generation XtruForm (XF-3) machine, adding controls and hardware that would be able to handle high strength sheet. They carried out three sets of trials using different sheet thicknesses of cryo-cooled (in LN2) sheets. PNNL assisted FT in developing the cryo-rolling process by performing a series of cryo-compression tests in combination with post-compression aging treatments and characterizing the resulting samples through hardness testing and microstructural analysis.

Technological problems, such as the rapid hardening of the sheet, necking type failure due to the relatively low stiffness of the rolling frame, warming up of the sheet during the rolling process, and knife-edging becoming exacerbated during cryo-rolling due to the surface layers warming up and becoming softer compared to the harder inside layers, limited the maximum strain that could be achieved to be below the targeted 80%. Based on the results to date in this work, the current processing conditions were able to match the existing strength but unable to exceed it.

Though the testing exposed several limitations of the planned experiments, the learning has been valuable. Future work should focus on continued cooling of the pre-cooled sheet while it is being rolled, and using a stiffer rolling frame with higher rolling force capability for increasing the rolling deformation beyond 30% without instability. Additionally, tension tests to directly evaluate the tensile yield and ultimate tensile strengths along with the tensile ductility are recommended.

Table of Contents

Introduction

High strength Al alloys being considered for automotive use typically belong to the 7xxx family with AA 7075 being the most common. AA7075 is a precipitation strengthened alloy with a tensile strength of ~600 MPa in its peak-aged temper (T6). However, steel industry has also come up with hot-stamping steels with strengths as high as 1.5-2 GPa (Usibor 1500P and 2000P of tensile strengths 1500 MPa and 2000 MPa, respectively). Therefore, lightweighting through material replacement (i.e. replace steel by Al), requires new approaches to go beyond the strength offered by precipitation strengthening in the 7xxx series alloys.

A survey of existing literature on fabrication of fine-grained materials shows that precipitation hardening aluminum alloys (such as AA7075) can be cryo-rolled and precipitation hardened to result in bulk nanocrystalline (NC) material with a desirable combination of properties [1] However, economical production of large quantities of NC (or nanostructured (NS)) materials has not yet been demonstrated. Ovidko et al. [2] state “Although these strategies are effective in providing concurrently high strength and high ductility in a large number of NS metallic materials, large-scale production of super strong NS materials with good ductility for various structural applications is still a challenge”. Therefore, there is a need for novel processes that can help realize the promise of NC/NS materials.

Stretch roll forming (SRF) technology is a patented technology developed by Fairmount Technology (FT) that has been shown to significantly cold work aluminum components. This work proposes to adapt FT’s SRF technology, in combination with cryo-rolling, to produce high strength nanocrystalline AA7075 sheet that is estimated to be 20% stronger than currently available 7075-T6, but equally formable. The key benefit of SRF is that it is already a relatively well-developed process, although it has not been used in combination with cryo temperatures. Therefore, this project will demonstrate suitability of cryo stretch roll forming for the high-strength AA7075 alloy and characterize the mechanical performance of the resulting product.

The target strength of the cryo stretch formed product is 700 MPa, that will be achieved through a combination of precipitation strengthening and nanocrystalline microstructure. If successful, a broad range of automotive components would be amenable to lightweighting by stamping out of a NC AA7075 sheet stock. Potential structural components that can benefit from this technology include impact beams, A and B-pillars, bumper beams, rails, etc. Thus, SRF technology is expected to have wide applicability to lightweighting multiple structural components, common to all vehicle makes and model, and whose geometry invariably requires plastic deformation to produce. Further, use of high-strength structural components may also lead to weight savings in secondary components.

Objectives

The two primary technical objectives of this project are:

1) Develop an Al 7075 sheet with 700 MPa strength

2) Achieve sufficient ductility and formability in the high-strength sheet suitable for stamping.

These objectives will be achieved through thermo-mechanical processing of AA 7075 material and developing processing-microstructure-property correlations. Specifically, cryo-rolling and stretch-forming approaches developed at FT will be used to impart large strains to develop nanostructured sheet that possesses the desired high strength and formability.

1.0 Experimental Approach

1.1 Rolling Trials

In preparation for rolling 7075-W sheets at cryogenic temperatures, Fairmount Technologies (FT) performed rolling trials on 7075-O sheets at room-temperature. Because 7075 is soft in the O temper, it was considered a reasonable surrogate for the similarly soft W temper. Rolling at room-temperature (instead of cryogenic temperatures) for the initial rolling trials was necessary for developing the rolling process and trouble-shooting the equipment without the additional complexity of maintaining cold temperatures. Further, the room-temperature rolling trials allowed FT to make mechanical adjustments to the hardware and to understand the load limits of their equipment. Process development at this stage will help develop rolling schedules for W temper sheets at liquid nitrogen temperatures.

Rolling trial #1 was conducted on Alclad 7075 sheets that was procured from Bralco Metals® in an O temper (7075-O). The sheet material had an initial thickness of 0.0625” (1.58 mm) and was sheared into strips 2.02” wide and 36” long. The rolling procedure for two of these sheets (sheet #3 and sheet #4) is listed in Table 1. Sheet #3 was successfully rolled 6 times to a final thickness of 0.0295” (0.75 mm, 53% thickness reduction). Sheet #4 was rolled 9 times to a final thickness of 0.0185” (0.47 mm, 70% thickness reduction) but broke during the final rolling pass.

Table 1. Rolling conditions for rolling trial #1 conducted at Fairmount Technologies.

Sheet (#)	Pass (#)	Starting Thickness (mm)	Ending Thickness (mm)	Thickness Reduction (%)	
				Pass	Cumulative
3	1	1.58	1.42	10.4	10.4
	2	1.42	1.32	7.14	16.8
	3	1.32	1.19	9.62	24.8
	4	1.19	1.04	12.8	34.4
	5	1.04	0.914	12.2	42.4
	6	0.914	0.749	18.1	52.8
4	1	1.58	1.40	11.7	11.7
	2	1.40	1.27	9.09	19.7
	3	1.27	1.14	10.0	27.8
	4	1.14	1.02	11.1	35.8
	5	1.02	0.876	13.8	44.6
	6	0.876	0.762	13.0	51.8
	7	0.762	0.648	15.0	59.1
	8	0.648	0.546	15.7	65.5
	9	0.546	0.470	14.0	70.3

Rolling trial #2 was performed on bare 7075 plate that was procured from Midwest Steel and Aluminum in a T651 temper and subsequently heat-treated to an O temper according to AMS 2770. The rolling procedure for the plate is listed in Table 2. The plate was rolled from an initial thickness of 0.25” (6.5 mm) to a final sheet thickness of 0.065” (1.65 mm, 75% thickness reduction) but fractured at several locations during this final pass.

Table 2. Rolling conditions for rolling trial #2 conducted at Fairmount Technologies.

Pass	Starting Thickness (mm)	Ending Thickness (mm)	Thickness Reduction (%)	
			Pass	Cumulative
1	6.50	6.50	0.00	0.00
2	6.50	5.64	13.3	13.2
3	5.64	4.52	19.8	30.5
4	4.52	4.27	5.62	34.4
5	4.24	3.25	23.4	50.0
6	4.52	3.51	22.5	46.1
7	3.51	3.51	0.00	46.1
8	3.51	2.39	31.9	63.3
9	2.39	1.65	30.9	74.6

For both rolling trials, sheets were rolled in multiple passes to reduce their thickness using Fairmount Technologies' stretch roll forming system SRF 1000. After each pass, a short section of sheet was cut off to produce specimens for characterization at PNNL (see Section 1.7).

A third set of trials were conducted using 3.26 mm thick starting sheet stock, heat treated to the W condition and cryo-cooled in LN2 prior to rolling. This set of tests presented a new problem, that as soon as the sheet got warmed up, the rollers would sink deep into the sheet and prevent the front tension from being able to pull the sheet through, causing the rolling process to stop.

1.2 Cryo-compression Tests

To assist FT with their rolling process, and to fabricate samples (with controlled deformation) for mechanical testing and microstructural analysis, cryo-compression tests were conducted at PNNL. Two different geometries of cylindrical specimens were prepared. For the "smaller" specimens, 12.7-mm-diameter cylindrical rods of 7075-T6 were cut into 25-mm-long specimens. For the "larger" specimens, 19-mm-diameter cylindrical rods of 7075-T6 were cut into 57-mm-long specimens. Both rod materials were purchased from McMaster-Carr. All the cylindrical specimens were then solution heat treated to a W temper at 480 °C for 65 min and then water quenched. Following quenching, the specimens were stored in a freezer at -60 °C to prevent natural aging.

A total of three sets of cryo-compression tests were conducted. The first and second sets of cryo-compression tests were conducted on the smaller 7075-W cylindrical specimens. The first set of experiments used an environmental chamber to compress specimens at -60 °C (see Figure 1a) and the second used a liquid nitrogen (LN) bath to compress specimens at approximately -196 °C (see Figure 1b). For these cryo-compression experiments, specimen dimensions were recorded before insertion into the load frame (while the specimen was at room temperature). A lubricant was applied to the loading faces of each specimen to reduce barreling due to friction. Specimens were compressed at an engineering strain rate of 0.05 s^{-1} (to mimic compressive loading during rolling) to either 5, 10, or 30% compressive strain, or until failure.

The third set of cryo-compression experiments were conducted on the larger 7075-W cylindrical specimens using a liquid nitrogen (LN) bath. Due to the requirement of higher deformation loads on account of larger specimen diameter, these experiments were conducted on a 500 kip load frame (see Figure 1c). A lubricant was applied to the platens on the load frame to reduce barreling due to friction. Specimens were cooled in a dewar filled with liquid nitrogen and then transferred to a liquid nitrogen bath on the test frame. The length and diameter of each specimen was measured as it was transferred to the test frame (i.e., after it had been cooled in

liquid nitrogen). Specimens were compressed at nominal engineering strain rate of 0.0083 s^{-1} (0.05 min^{-1}), i.e. a slower strain rate than the before, to ensure the cylinders were strained uniformly, to either 10%, 20%, or 30% total strain.

Axial compressive strain was calculated using crosshead displacement; therefore, compliance was corrected using the temperature-dependent elastic modulus of aluminum. Flow stress and maximum strain before failure were measured and provided to FT to help design and size their cryo-rolling system.

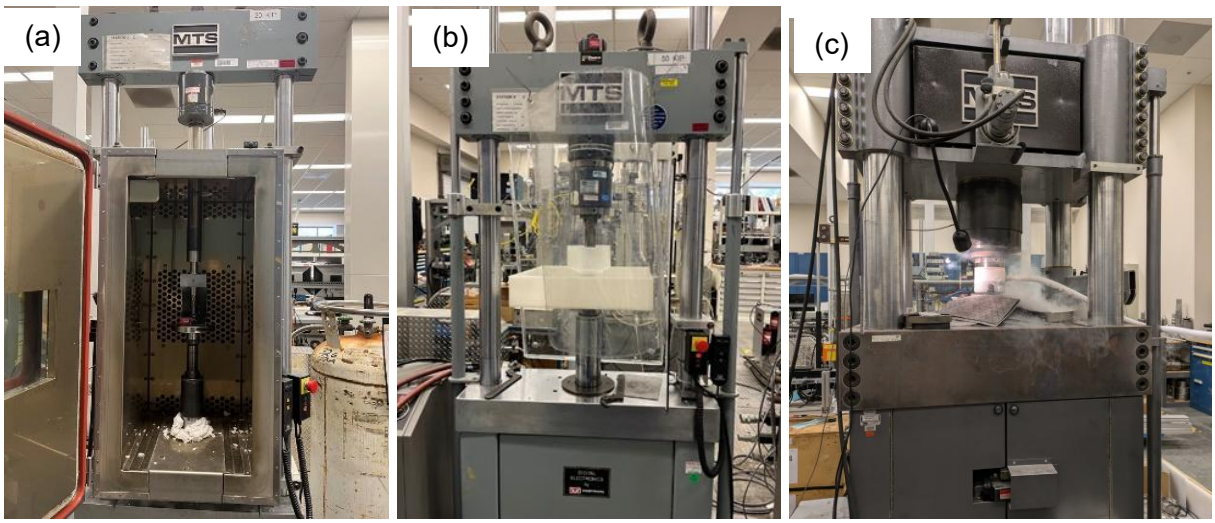

Fig. 1 PNNL's mechanical test capabilities showing the (a) environmental chamber and (b) liquid nitrogen (LN) bath setup used to conduct cryo-compression tests on the "smaller" diameter specimens and (c) the LN bath setup used to conduct cryo-compression tests on the "larger" diameter specimens. Source: PNNL

1.3 Natural Aging Tests

Unrolled 7075-O plate from rolling trial #2 (6.5 mm thick) was shipped to PNNL to study the stability of the W temper. The plate was solution treated at 480°C for 65 min and then water quenched at room-temperature (RT) to produce a W temper. The plate was then allowed to naturally age at room temperature for up to 11 days. Rockwell B hardness was measured at periodic intervals to monitor hardness evolution in the plate.

To investigate the effect of cryo-compression on natural aging, specimens of 7075-W were cryo-compressed to 20% strain at -196 °C, sectioned in half, and allowed to naturally age at room temperature for up to 9 days. Rockwell B hardness was measured at periodic intervals to monitor hardness evolution in the compressed cylinders.

1.4 T6 Heat Treatment

To investigate the effect of cryo-compression on the evolution of peak strength in 7075, specimens of 7075-W were cryo-compressed at -196 °C to strains ranging from 5 to 60 % and then artificially aged. Artificial aging was conducted at 120 °C using a Vulcan tabletop box furnace in an air environment for times ranging from 2 to 12 hours. Rockwell B hardness was measured after artificial aging as a surrogate for measuring tensile strength.

1.5 Tensile Tests

To investigate the effects of cryo-compression on strength and ductility in Al 7075, tensile specimens were prepared from the “larger” Al 7075 specimens that had been cryo-compressed to various strains (see Section 1.2) and heat treated to a T6 temper at 120 °C for 24 hours (*i.e.*, machining was done after the specimens were T6 aged). The initial cylindrical specimens could only be cryo-compressed up to a maximum compressive strain of 30% such that the final cylinder’s length was sufficient to extract tensile specimen from. Compressive strains beyond 30% would lead to barreling i.e. non-uniform deformation, making it difficult to machine tensile samples with homogeneous pre-deformation. The geometry of the tensile specimens is approximately proportional to the standard ASTM E8 geometry for round specimens and features a double-shoulder design for gripping and loading the specimens in uniaxial tension until rupture, see Figure 2. The specimens were oriented so that their tensile loading axis was parallel to the loading axis during cryo-compression. The diameter of the gage region was 1.8 mm and the gage length was 9 mm. Specimens were loaded in uniaxial tension until rupture at a constant engineering strain rate 0.01 s^{-1} and strain was measured using an optical extensometer.

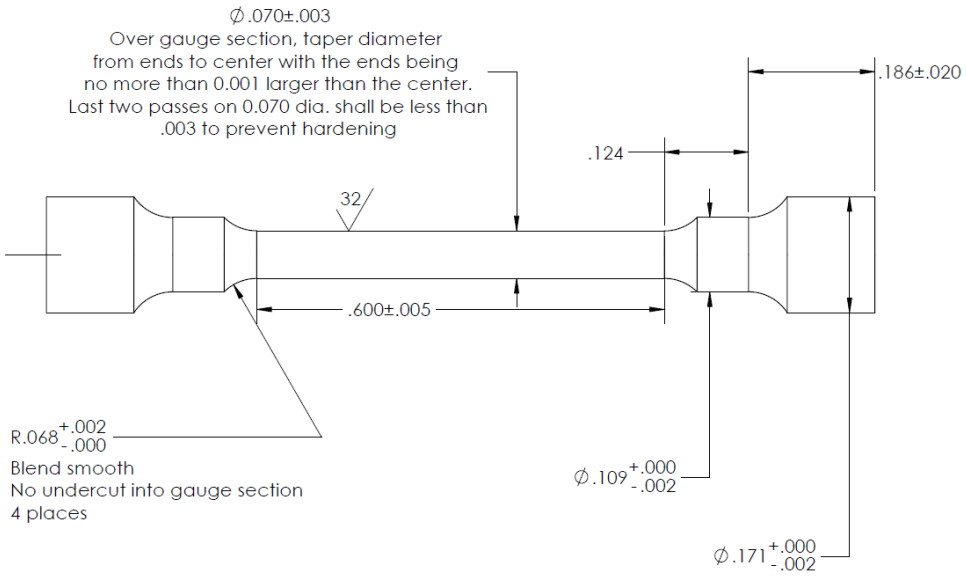

Fig. 2 Geometry of the tensile specimens (all dimensions are in inches).

1.6 Corrosion Tests

To study the effect of cryo-compression on corrosion behavior, open circuit potential (OCP) and potentiodynamic polarization (PD) tests were performed. Specimens were prepared from 7075 rod material in the following conditions: O, T6, T7, and cryo-compression + T6. The O temper was produced by annealing at 410 °C for 3 hours then air cooling, the T6 temper was produced by solution heat treating (480 °C for 65 minutes → water-quench) and artificially aging at 120 °C for 24 hours, and the T7 temper was produced by solution heat treating (480 °C for 65 minutes → water-quench) and artificially aging at 175 °C for 10 hours, all in accordance with the ASM handbook for 7075 rod material. The cryo-compressed specimen was solution heat treated (480 °C for 65 minutes → water-quench), cryo-compressed to 30% compressive strain, then artificially aged with T6 heat treatment of 120 °C for 24 hours. Specimens were sectioned, mounted in epoxy, and polished to a final polish with 1 µm diamond polish.

Specimens were mounted onto PNNL's "home-built" multimodal corrosion system shown in Figure 3. Electrical connection to the specimen was made through a rod threaded into the rear of the epoxy mount of each specimen. A saturated calomel electrode was used as the reference electrode and graphite rods were used as counter electrodes. The reference electrode was placed at less than 1 mm from the sample. For each specimen, the OCP test was first conducted over a measurement duration of 1800 s (30 minutes). The PD measurement was then performed at a scan rate of 10 mV/min over a potential range of -200mV vs OCP to -400 mV vs SCE. A high-resolution camera with a Tokina atx-i microlens was used to capture photographic images of the specimen surface during the corrosion tests.

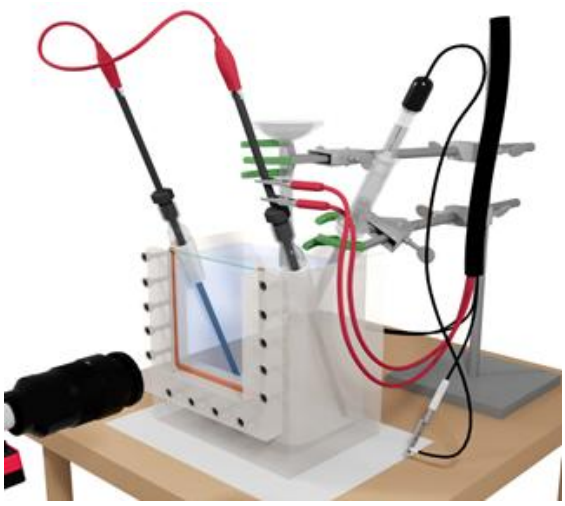

Fig. 3 Schematic showing the bulk electrochemical/multimodal corrosion system used to conduct open circuit potential (OCP) and potentiodynamic polarization (PD) tests. Source: PNNL

1.7 Microstructural Characterization

To study the effect of rolling on the Al 7075 sheet, metallographic specimens (provided by FT) were sectioned from unrolled and rolled sheet specimens along the rolling direction (RD) and long transverse direction (LTD). The specimens were mounted in epoxy and polished for subsequent optical microscopy (OM) and scanning electron microscopy (SEM). Electron back scattered diffraction (EBSD) was conducted on unrolled, 6.5-mm-thick 7075-O plate that was solutionized and allowed to naturally age to a stable, T4 temper to further investigate the grain size through the thickness of the plate.

To study the effect of cryo-compression on Al 7075 rod, metallography specimens were prepared from uncompressed rod material and rod that was compressed to 30% strain. Both specimens were sectioned to reveal the axial face, mounted, polished, and etched to reveal grains with a polarized light filter.

2.0 Results & Discussion

2.1 Rolling Trials

During the rolling trials at FT, hardness data was collected from specimens after various amounts of cumulative thickness reduction. These hardness data are shown in Figure 4. As a reminder, sheet #3 was rolled to a final thickness reduction of 53% in 6 passes and sheet #4 was rolled to a final thickness reduction of 70% after 9 passes. After 4 passes, both sheets had a similar thickness reduction (~35%), but sheet #3 had significantly higher hardness than sheet #4. It should be noted, however, that the hardness data for sheet #4 at this strain level was measured with 0.5 kgf load, whereas all the other data were collected with 1 kgf load. The final hardness of sheet #4 was 24% greater than the final hardness of sheet #3, which is expected since it experienced more severe thickness reduction.

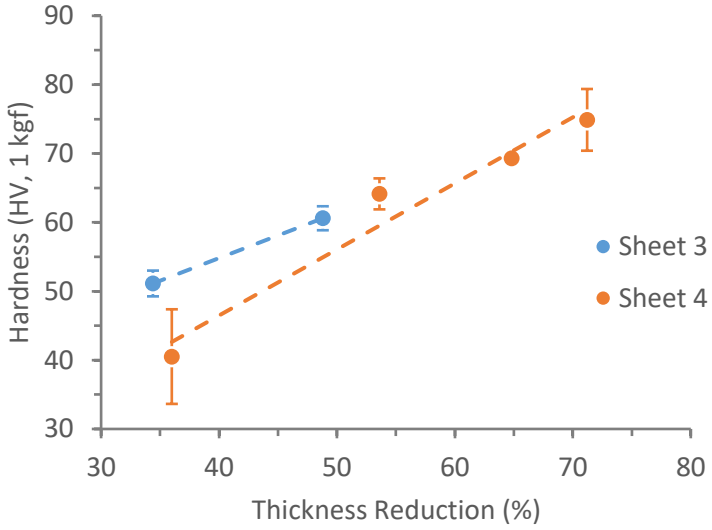

Fig. 4 Vickers hardness measured during the rolling experiments plotted as a function of cumulative thickness reduction. Source: PNNL

2.2 Cryo-compression Tests

The stress-strain curves from compression tests at room-temperature (RT) and -60 °C are presented in Figure 5. The RT tests demonstrate serrated yielding or Portevin-Le Chatelier (PLC) effect beyond 8% crosshead engineering strain whereas tests at -60 °C did not.

Representative stress-strain curves from cryo-compression tests conducted at liquid nitrogen (LN) temperature are presented in Figure 6. Some tests were interrupted at nominal strains of 5, 10, 20, and 30% while the other tests were conducted until the specimens failed. All the stress-strain curves align with each other showing good repeatability. Specimens could be compressed to strains of nearly 60% (flow stress ~1150 MPa) without fracture, implying good compressive ductility of 7075-W at LN temperature. The flow stresses and maximum compressive strains observed during LN tests are larger than those observed during compression tests at warmer temperatures of 25 and -60 °C (see Figure 5). Greater ductility at LN (relative to -60 °C) has

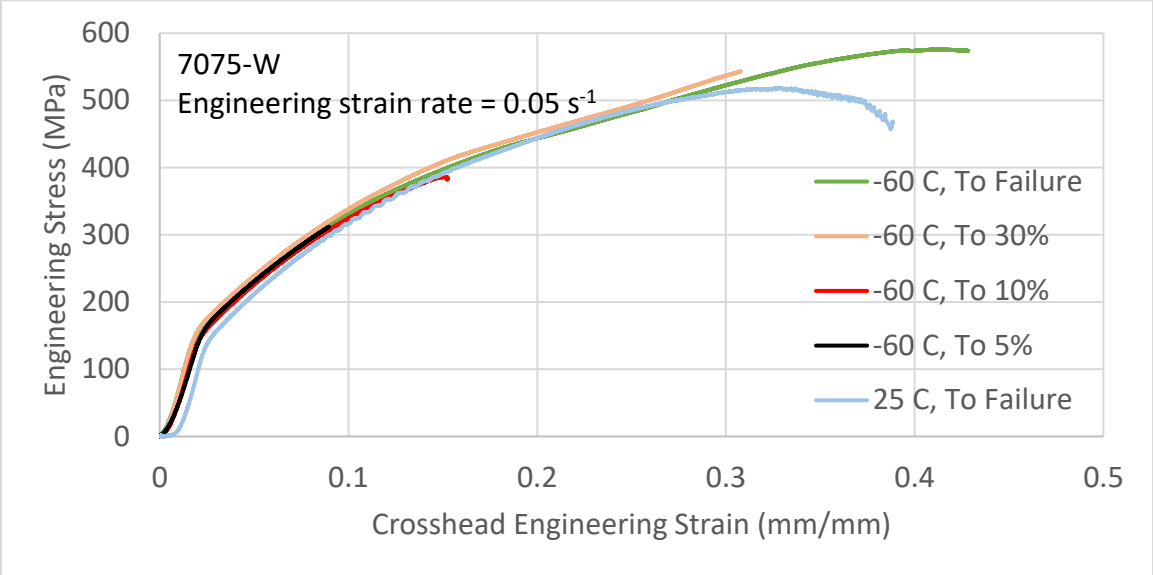

Fig. 5 Representative stress-strain curves from compression tests conducted on 7075-W at room-temperature (RT) and -60 °C. Source: PNNL

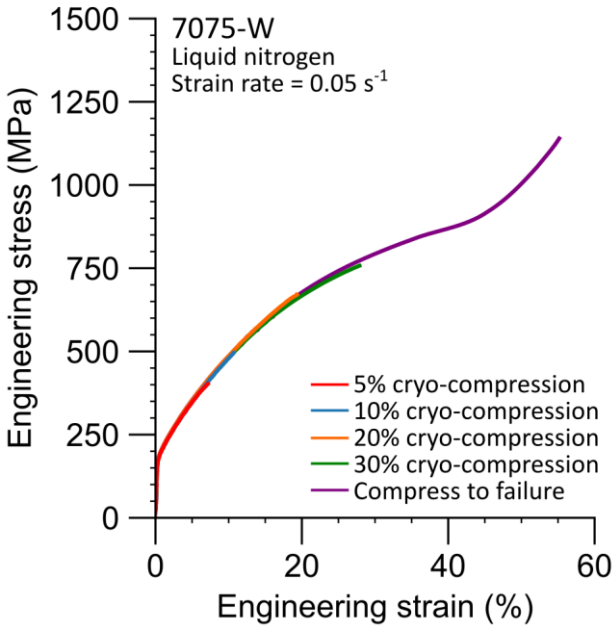

Fig. 6 Representative stress-strain curves from cryo-compression tests conducted on 7075-W at -196 °C (liquid nitrogen (LN)). Source: PNNL

been attributed to the high stacking fault energy of 7075 and the suppression of dynamic recovery at LN temperatures [3].

Cylindrical specimens (diameter 19 mm) of 7075-W were compressed to 10, 20, and 30% strains at LN temperature at a nominal engineering strain rate of 0.05 min^{-1}, or 0.00083 s^{-1}. This strain rate, which is slower than the other cryo-compression experiments, was chosen to ensure

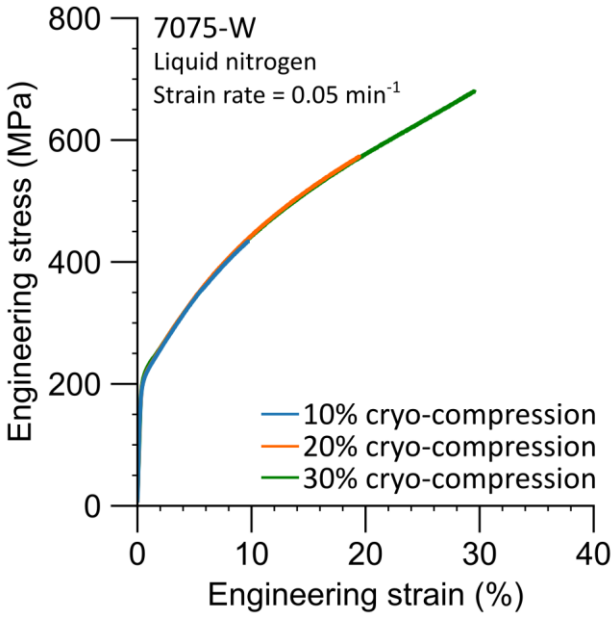

Fig. 7 Representative stress-strain curves from cryo-compression tests conducted on 19-mm-diameter cylinders of 7075-W at -196 °C (liquid nitrogen) in preparation for tensile tests. Source: PNNL

good repeatability between all tests. Indeed, the residual compressive strain of all specimens (taken from physical measurements of the specimens before and after compression) was within 1% of their target strain. The slower strain rate was also chosen to help ensure the specimens strained uniformly, as the compressed specimens were later used to produce tensile specimens. Representative stress-strain curves of the specimens during compression are shown in Figure 7. There is good overlap between all the stress-strain curves, demonstrating the reproducibility of the data. The engineering stresses are slightly less than the stresses observed at the faster strain rate (0.05 s^{-1}, see Figure 6), indicating that the material flow behavior may be sensitive to strain rate at cryogenic temperatures.

2.3 Natural Aging Tests

To test the stability of the W temper, 6.5-mm-thick plates of 7075 were solutionized (480 °C for 65 min → water quench) and allowed to naturally age at room temperature. Figure 8 shows the hardness evolution of the plate over 11 days (267 hr.). Hardness increases almost immediately due to natural aging after quenching, increasing by 18% (from 51 HRB to 60 HRB) in just 4 hours. After 18 hours of natural aging, the hardness increased to 72 HRB (41% increase from the initial solutionized condition). The hardness of the material plateaued at 80 ± 2 HRB after ~4 days of natural aging (91 hours) and reached a maximum hardness of 82 ± 1 HRB after 11 days of natural aging. In previous studies, the hardness increase during natural aging of 7xxx-series aluminum alloys has been attributed to solute clustering and GP zone formation. The rapid increase of hardness during the first few hours of natural aging suggests that these nano-scale features (*e.g.*, GP zones) form very quickly. Therefore, to preserve the microstructure of 7075 in

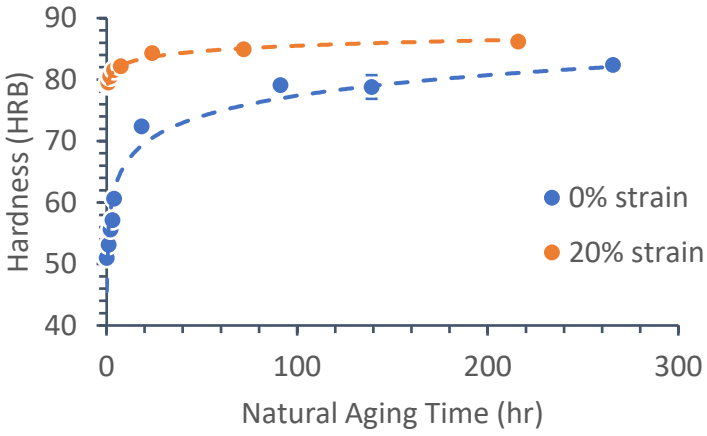

Fig. 8 Hardness evolution in 7075 during natural aging after a solution heat treatment with no compression (plate material) and after 20% cryo-compression (rod material). Source: PNNL

the W temper, care must be taken to minimize the time at room temperature when preparing metallography specimens.

To study the effect of cryo-compression on natural aging, specimens of 7075-W that had been cryo-compressed to 20% strain in liquid nitrogen were allowed to naturally age. The initial hardness just after cryo-compression (79 ± 1 HRB) was equal to the hardness of the uncompressed plate material that was naturally aged for 91 hours. While the hardness of the cryo-compressed material did not increase as significantly as the uncompressed material, it plateaued at a hardness of 85 ± 1 HRB after only 24 hours of natural aging. This suggests that cryo-compression accelerates natural aging, which could be the result of dislocations, generated during cryo-compression, accelerating the nucleation of η precipitates.

2.4 T6 Heat Treatment

After cryo-compression in liquid nitrogen, specimens of 7075-W were artificially aged at 120 °C to produce a T6 temper condition. Rockwell B hardness is plotted as a function of aging time in Figure 9 for specimens that were cryo-compressed with various strains from 0 to 60%. Cryo-compression (prior to artificial aging) was able to drastically increase hardness. The as-compressed hardness of the specimen compressed to 60% strain was double that of 7075-W (no compressive strain). The increase in hardness (strength) can be attributed to strain hardening during cryo-compression. Further, the application of compressive strain also reduced the aging time required to achieve T6 hardness. For example, the application of 60% compressive strain halved the time needed to reach 95% of the T6 hardness from 6 hours to 2.7 hours. This reduction in aging time could be the result of enhanced nucleation, with dislocations from cryo-compression serving as heterogeneous nucleation sites for η' precipitates.

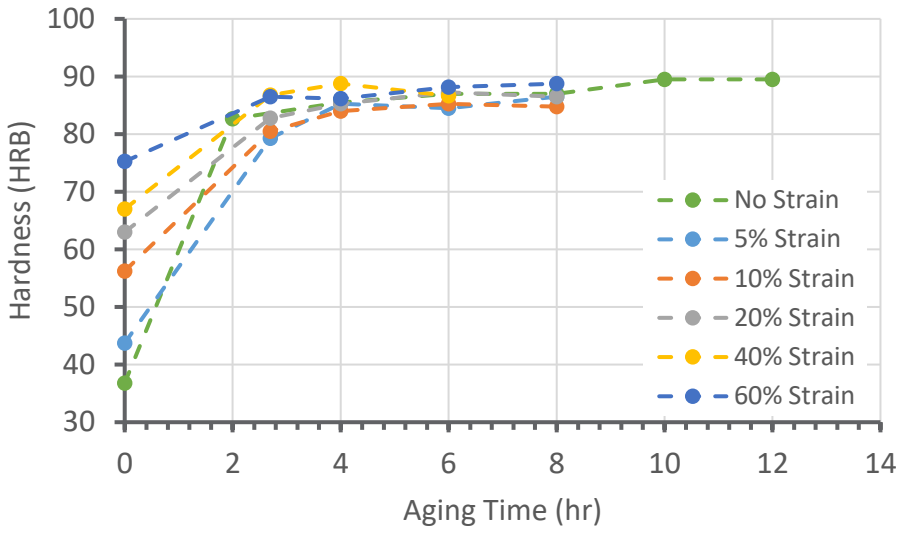

Fig. 9 Rockwell Hardness B scale measurements for samples compressed under liquid nitrogen and heat treated at 120 °C. Source: PNNL

Microhardness specimens were prepared from 7075-T6 uncompressed material and from material compressed at -196 °C. Figure 10 presents microhardness maps measured from the 13-mm-diameter specimens and Figure 11 presents microhardness maps measured from the 19-mm-diameter specimens. The microhardness maps in Figure 10 show that both the uncompressed (Figure 10a) and compressed (Figure 10b) specimens have greater hardness along a 45° relative to the length of the original rod (which is the same axis the material was compressed along). The greater hardness along a specific direction could be attributed to greater deformation along the plane of maximum shear which is oriented at 45° relative to the loading axis. However, the reason for greater hardness along the 45° direction in an undeformed specimen is not clear and it may have been inherited from the fabrication process of the rods themselves. The uncompressed sample has a slightly greater hardness along the 45° diagonal, but the transition in hardness between the regions of high and low hardness is more gradual. Interestingly, microhardness measured from the larger-diameter specimens (whether undeformed or compressed to 30% strain) did not observe this greater hardness along the 45° angle, as shown in Figure 11. Rather, microhardness was fairly uniform across the axial surfaces of the larger-diameter specimens. Therefore, it is likely that the greater hardness along the plane at 45° to the long axis of the cylindrical specimens (13 mm diameter) may have been inherited from the as-fabricated rods themselves.

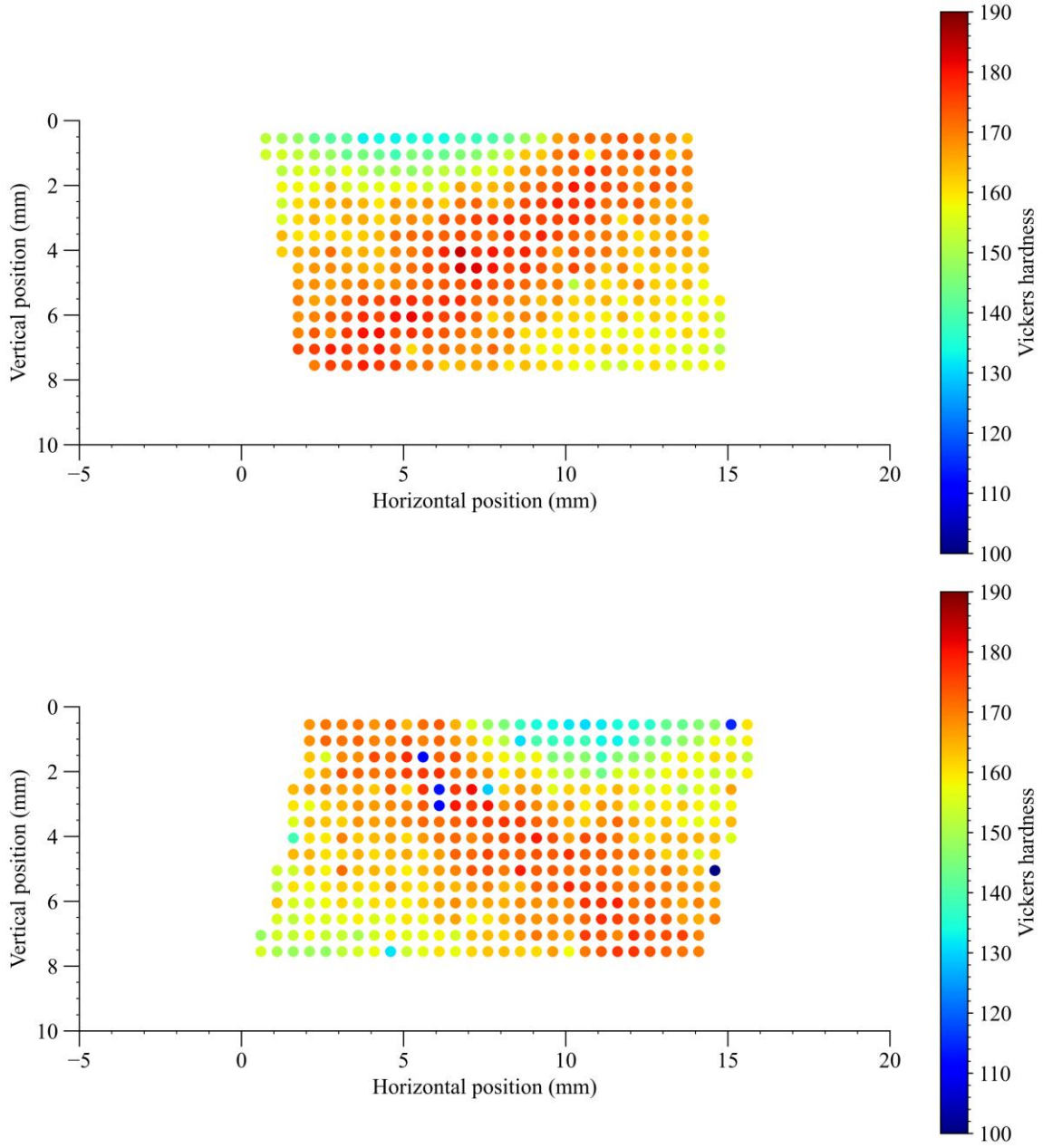

Fig. 10 Vickers microhardness across the longitudinal cross section of a) an uncompressed specimen of 7075-T6 and b) a specimen compressed to 60% strain under liquid nitrogen. Both specimens were prepared from 13-mm-diameter rod material. The compressive direction and cylindrical long axis are along the vertical axis of the plots. Source: PNNL

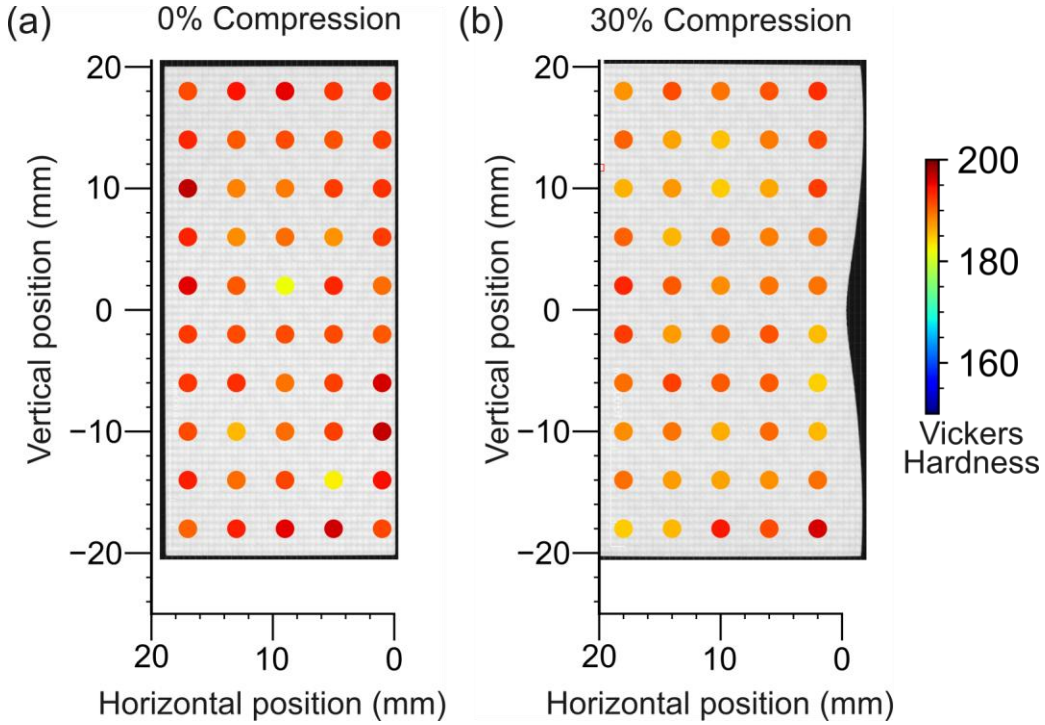

Fig. 11 Vickers microhardness across the longitudinal cross section of (a) an uncompressed specimen of 7075-T6 and (b) a specimen compressed to 30% strain under liquid nitrogen and artificially aged with a T6 heat treatment. Both specimens were prepared from 19-mm-diameter rod material. The compressive loading axis and longitudinal axis of both specimens are along the vertical direction. Source: PNNL

2.5 Tensile Tests

Cylindrical, shoulder-loaded tensile specimens were machined from specimens of 7075-W that were cryo-compressed at -196 °C and heat treated to a T6 temper at 120 °C for 24 hours. Representative tensile curves from artificially aged T6-temper specimens, which had been previously cryo-compressed to 0%, 10%, 20%, and 30% strain in W temper, are shown in Figure 12. Table 3 summarizes the average tensile properties. The cryo-compressed specimens exhibit lower yield strength, uniform elongation, and total elongation than the specimens that received no cryo-compression. These lower tensile properties in pre-cryo-compressed specimens may be the result of the cryo-compressed specimens being in an over-aged condition despite being given the standard T6 treatment. Essentially, cryo-compression introduced a high dislocation density in the W temper specimens such that upon subsequent T6 treatment, the kinetics of precipitation hardening would have been accelerated significantly (as was previously discussed in Section 2.4). Since the T6 treatment duration was kept the same as for un-compressed specimens (120 °C, 24 hours), the pre-compressed specimens likely continued to age past their peak strength and ended up with an overaged temper.

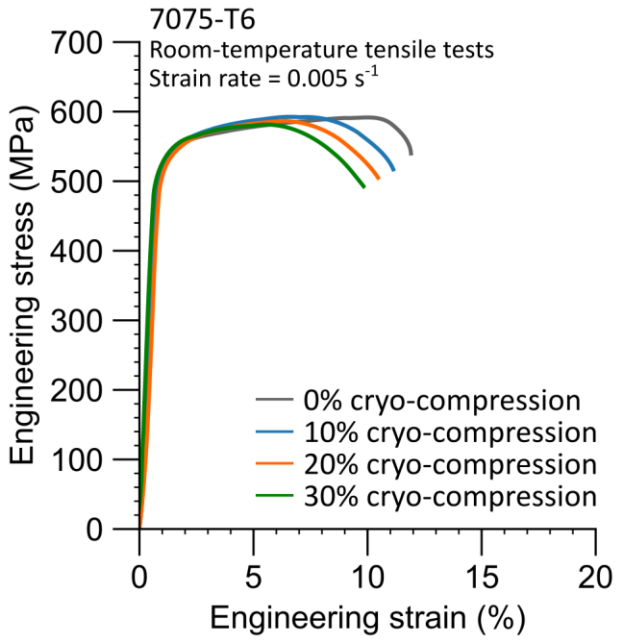

Fig. 12 Representative room temperature tensile stress-strain curves measured from specimens of 7075 that were solution heat treated, cryo-compressed, and then artificially aged with a T6 heat treatment. Source: PNNL

Table 3. Average tensile properties measured from specimens of 7075 that were solution heat treated, cryo-compressed, and then artificially aged with a standard T6 heat treatment.

Cryo-Compression (%)	# of specimens	YS (MPa)	UTS (MPa)	e_{total} (%)
0	4	518 ± 7	595 ± 11	11.7 ± 2.7
10	4	507 ± 5	589 ± 5	10.7 ± 0.7
20	4	501 ± 10	584 ± 7	10.5 ± 0.8
30	4	503 ± 12	583 ± 5	10.4 ± 0.5

To better demonstrate the effect of cryo-compression in W temper on T6 temper strength, YS and UTS are plotted as a function of cryo-compression strain in Figure 13. While the differences in YS and UTS from 10 to 30% compressive strain are not statistically significant, applying any amount of cryo-compressive strain decreases YS and UTS by 3 and 2%, respectively. This decrease in strength with increasing amounts of cryo-compression suggests that the cryo-compressed specimens were overaged during the T6 aging treatment. According to the heat treatment study in Figure 8, cryo-compression reduced the amount of artificial aging required to reach 95% T6 hardness from ~6 hours to ~3 hours. However, all the tensile specimens received the same artificial aging heat treatment of 120 °C for 24 hours. If cryo-compression accelerates the nucleation of η' precipitates, then it is possible that the cryo-compressed specimens may have slightly overaged compared to the specimens that did not receive any cryo-compression.

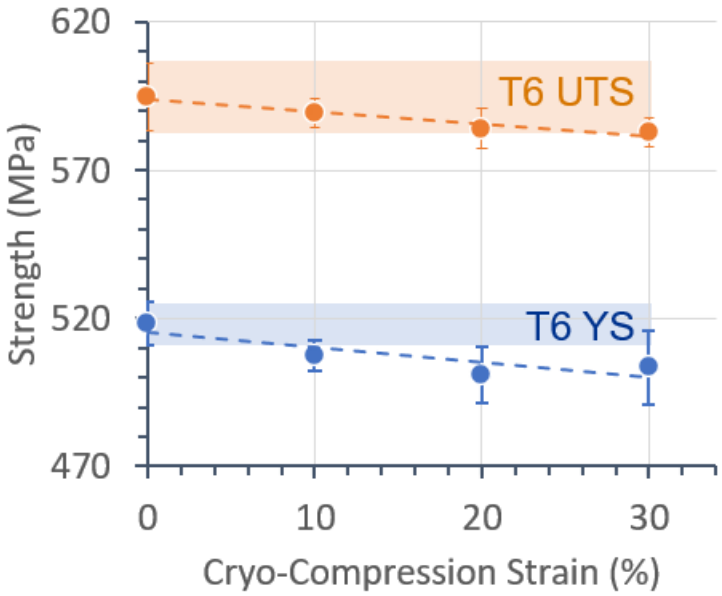

Fig. 13 Yield strength (YS) and ultimate tensile strength (UTS) plotted as a function of cryo-compression strain applied before a T6 heat treatment of 120 °C for 24 hours. The blue and orange bands represent the T6 YS and UTS, respectively, within 1 standard deviation. Source: PNNL

2.6 Corrosion Tests

Corrosion tests were conducted on 7075 rod material in three tempers (O, T6, and T7) as well as material that was cryo-compressed to 30% strain in W temper and then heat treated with a standard T6 treatment (120 °C, 24 hr.). The open circuit potential (OCP) curves are shown in Figure 14a and the potentiodynamic (PD) curves are shown in Figure 14b. The OCP plot shows the O temper- AA7075 sample to have the most negative OCP value stabilizing at approximately -860 mV vs SCE. The other materials exhibit a narrow range of stabilized OCP values ranging between -805 mV to -815 mV vs SCE, with the OCP of T73 greater (more positive) than T6-cryo compressed, greater than T6 condition.

Figure 14(b) shows the PD plot of the AA7075 samples investigated in this study. The O temper had the most negative corrosion potential (Ecorr) compared to the other conditions at -851 mV, indicating it has the greatest readiness to participate in a corrosion reaction. The T73 temper condition showed an Ecorr of -792 mV, indicating it is more noble relative to other tempers used here. This is expected as the T73 condition, also known as the overaged condition, was developed to increase the stress-corrosion-cracking resistance of 7075 albeit with some loss of strength compared to the T6, or peak aged, condition. There was no difference in PD behavior between the T6 and the cryo+T6 conditions. The T6 and cryo+T6 conditions also show a characteristic breakdown potential at ~ -750mV vs SCE that is seen for peak aged AA7XXX alloys. This breakdown potential is associated with the breakdown of a protective hydroxide film that forms and covers the surface during the anodic polarization of the material. This film breakdown is accompanied by significant hydrogen evolution and pitting. With increase in applied potential, pitting occurs across the sample, thereby releasing significant hydrogen bubbles.

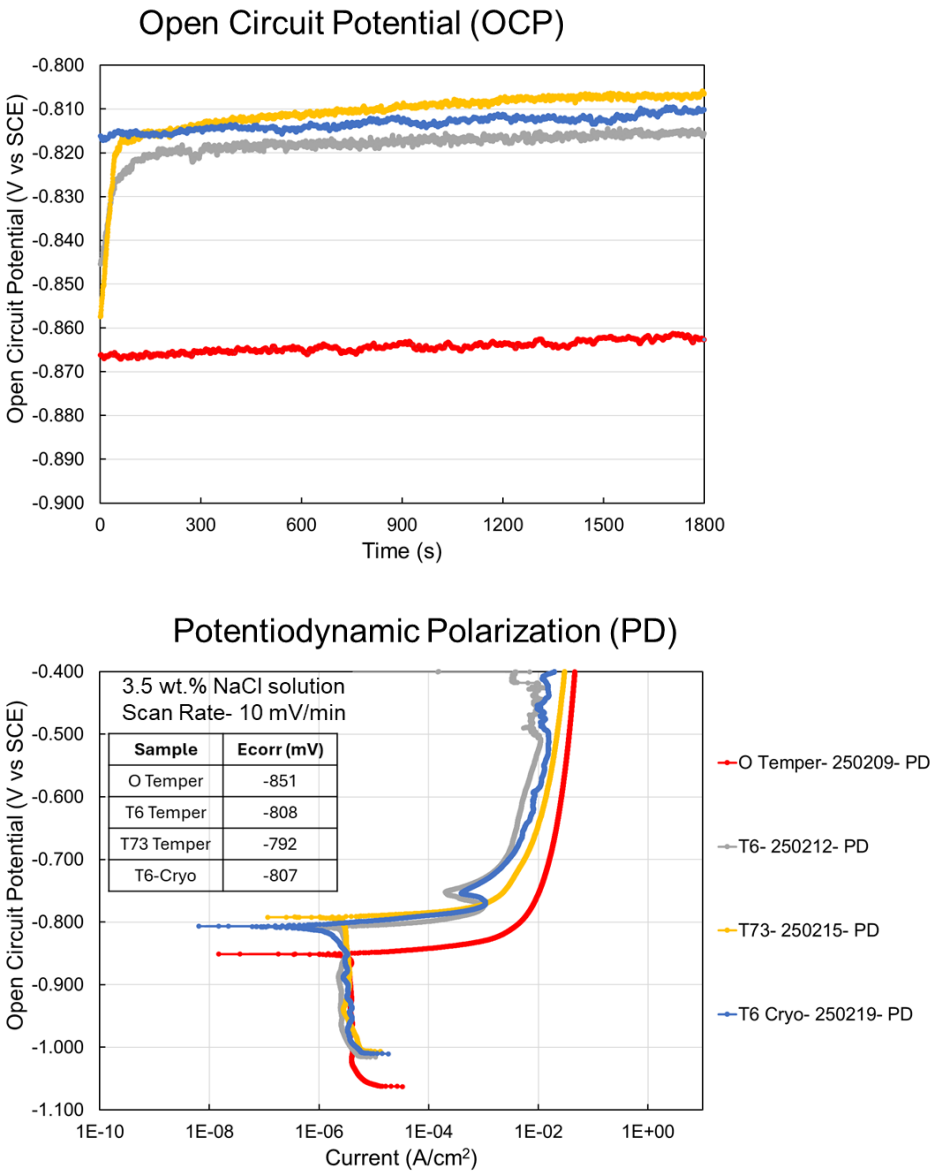

Fig. 14 (a) Open circuit potential and (b) potentiodynamic polarization curves for 7075 in the O, T6, T73, and CC+T6 (30% cryo-compression + T6 heat treatment) conditions. Source: PNNL

2.7 Microstructural Characterization

2.7.1 Rolling Trials

The optical micrographs in Figure 15 depict various orientations of the grains along the top surface (RD-LT), through-thickness along the rolling direction (RD-ST), and through-thickness along the long transverse direction (LT-ST) of unrolled 7075-T4 sheet material. The grains are elongated along the rolling direction and have a pancake-like morphology, which is typical of rolled sheet and plate, and is likely the result of the plate production process. The through-thickness sections show that the grains are thinner and more elongated at the center of the plate thickness than near the edge of the plate.

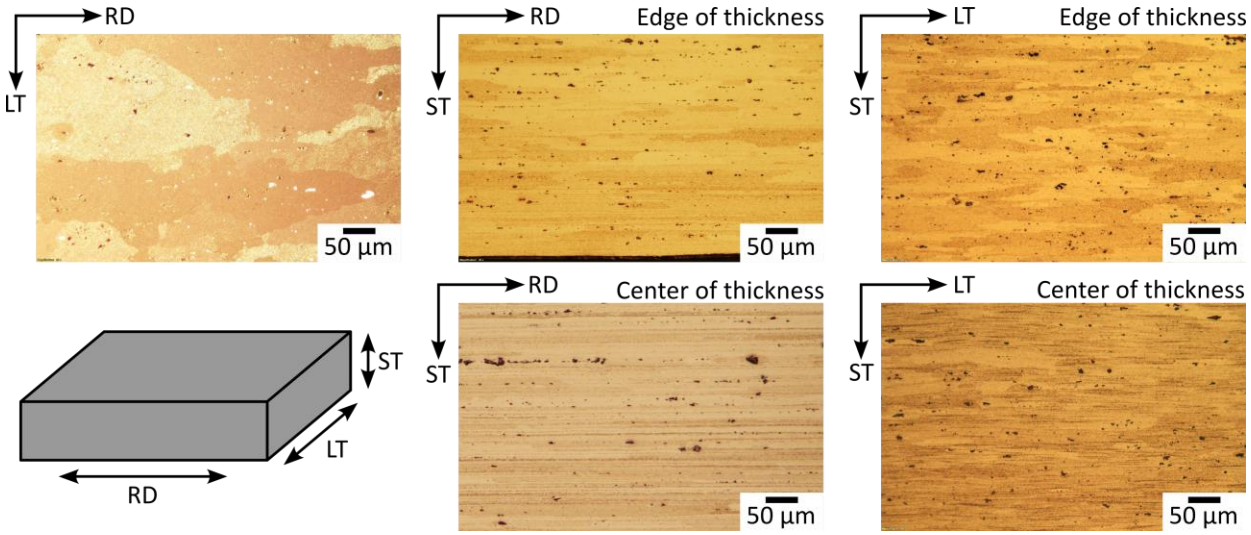

Fig. 15 Optical images of the solution treated, water quenched, and naturally aged 7075 sheet along three directions. RD = rolling direction; ST = short transverse; LT = long transverse. Source: PNNL

To more accurately quantify the difference in grain thickness at the center of the plate versus the edge of the plate, EBSD was conducted. Figure 16 shows inverse pole figure maps (IPF-Z) of the RD-ST cross-section (*i.e.*, through-thickness along the rolling direction). Maps were generated near the edge of the plate thickness and near the center of the plate thickness. The color-coded EBSD maps confirm that the grains are highly elongated along the rolling direction and highlight the gradation in grain thickness, with thinner grains at the center. The area-weighted average thickness of the grains (thickness is defined as the minor diameter of the ellipse fit to each grain) is 29 ± 10 um near the edge of the plate and 15 ± 3 um at the center of the plate. The regions near the edge of the plate also had more high angle grain boundaries compared to the center of the plate thickness. Near the edge of the plate thickness, ~84% of the grain boundaries had misorientation of over 10° whereas 68% of the grain boundaries at the center of the plate thickness had a misorientation of over 10°.

Figure 17 shows SEM micrographs of specimens from rolling trial #2 that were rolled to 0% (i.e. unrolled), 34%, and 75% thickness reduction strains, respectively. The unrolled, heat-treated sheet (see Figures 17a, d) had an inhomogeneous distribution of precipitates/intermetallic particles throughout the material. Some regions had a high concentration of larger precipitates (marked with yellow arrows) whereas other regions had fewer or no apparent precipitates (marked with red arrows). After rolling to 34% thickness reduction strain (see Figures 17b, e), the precipitates appeared to be aligned along the rolling direction. After rolling to high thickness reduction strains of 75% (see Figures 17c, f), most of the larger precipitates appear to be broken down and distributed homogenously although some large precipitates/intermetallic particles remain (indicated by yellow arrows).

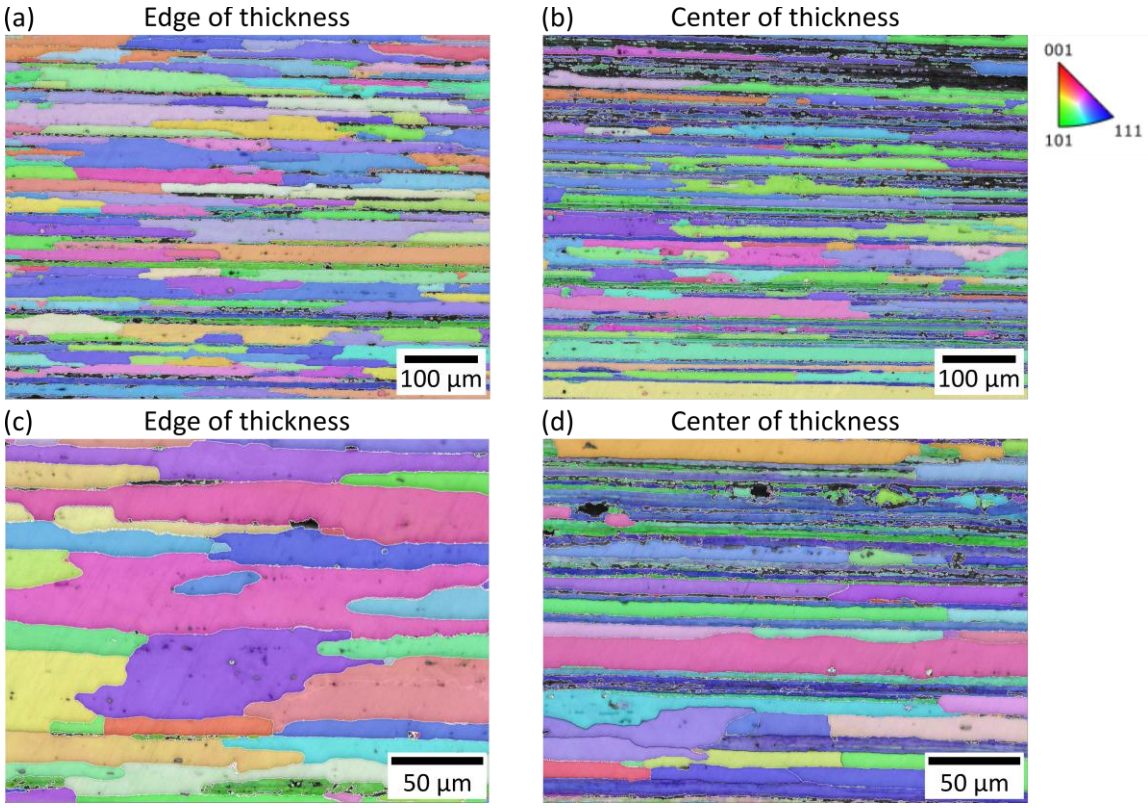

Fig. 16 EBSD Inverse Pole Figure – Z map from (a, c) the edge and (b, d) the center of the plate thickness in the RD-ST cross-section at (a, b) lower magnification and (c, d) higher magnification. Source: PNNL

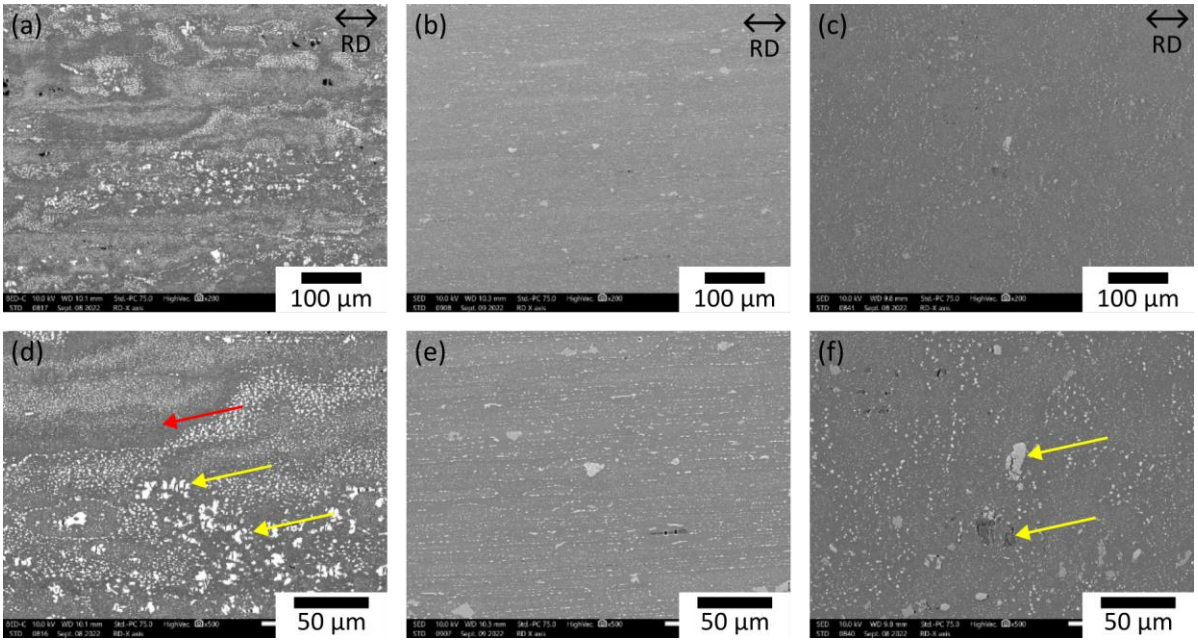

Fig. 17 Low magnification (a-c) and higher magnification (d-f) SEM micrographs depicting the precipitates in (a, d) unrolled sheet, (b, e) sheet rolled to 34% thickness strain, and (c, f) sheet rolled to 75% thickness strain. Source: PNNL

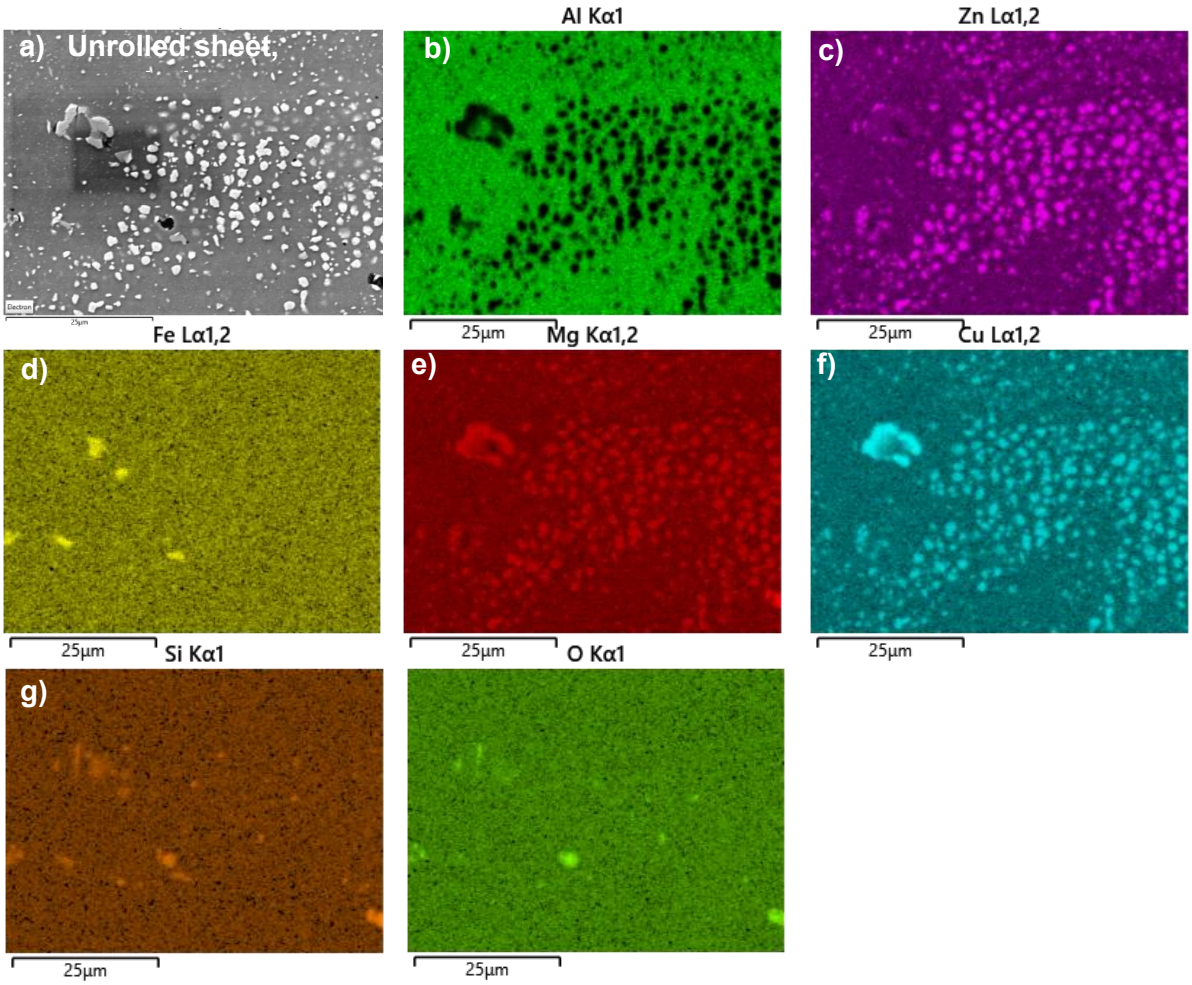

Fig. 18 Energy Dispersive Spectroscopy (EDS) map of unrolled sheet from experiment #2 showing a) Secondary electron (SE) image b) Al map c) Zn map d) Fe map e) Mg map f) Cu map g) Si map and h) O map. Source: PNNL

Figure 18 depicts EDS maps of the unrolled sample from rolling trial #2, with Al, Zn, Fe, Mg, Cu, and Si mapped. Most of the secondary phases (which appear white in Figure 18a) consist of Mg, Zn, and Cu which could be coarse η-phase (Mg $(Zn, Cu)_2$). There are some instances of Fe-rich precipitates (see Figure 18d), which could be Al_7Cu_2Fe. Some Si-rich precipitates were also observed (see Figure 18g) which could be SiO_2.

Figure 19 compares specimens from rolling trials #1 and 2 that had similar thickness strains of ~35%. Both sheet materials have a somewhat even distribution of secondary phases (i.e., there are no precipitate-free zones), but the morphology and alignment of the precipitates are different. The precipitates are randomly distributed throughout the sheet from rolling trial #1 (see Figure 19a) whereas the precipitates in the sheet from rolling trial #2 (Figure 19b) are aligned along the sheet rolling direction (RD). Furthermore, the precipitates from rolling trial #1 are round while the precipitates from rolling trial #2 appear to be elongated in a direction parallel to the rolling direction. There are a few possible explanations for these differences in precipitate distribution and morphology. First, the sheet materials from rolling trial #1 and #2 were procured from different sources and therefore have slightly different chemistries. Second, the sheet material from rolling trial #2 was received in the T651 temper and was subjected to additional

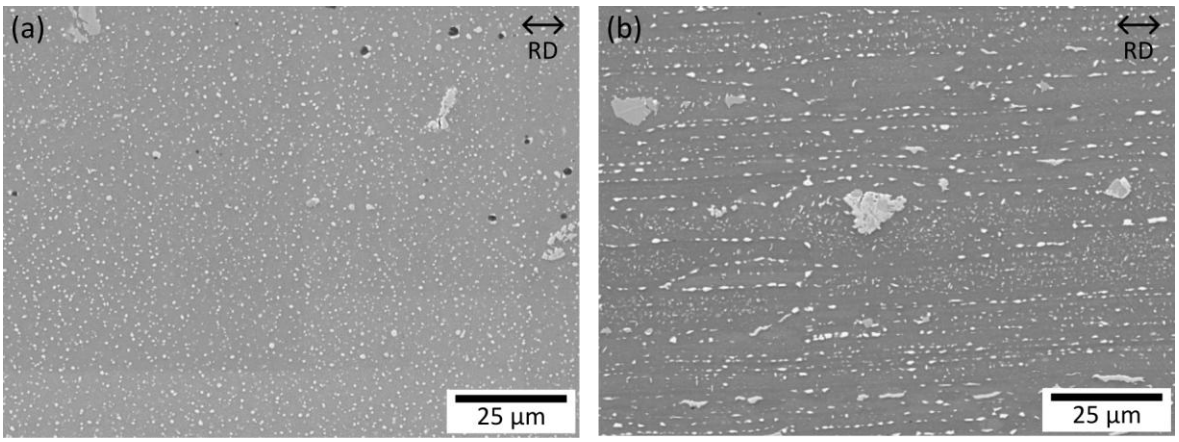

Fig. 19 SEM micrographs from (a) rolling trial #1 and (b) rolling trial #2 after both sheets were rolled to similar thickness strains (36 and 34%, respectively). Source: PNNL

thermal treatments to produce the O temper, whereas the sheet material from rolling trial #1 was procured in the O temper.

2.7.2 Cryo-Compression

Figure 20 compares optical micrographs of 7075 rod material with no cryo-compression and with 30% cryo-compression. The grains in the uncompressed rod (see Figure 20a) are elongated along the length of the rod (indicated by a red dot-dash line), which is expected for extruded material. The grains in the cryo-compressed rod (see Figure 20b) are still elongated, but the orientation of the grains (indicated with dashed brown lines) varies with location. The shape of the compressed specimen, with lateral deflection towards the left, indicates that the specimen buckled. The direction of the grains follows this buckled shape, sharply bending towards the left on the right side, and transitioning to a more gradual bend on the left side. Despite this, the grains at the center of the specimen, where tensile specimens were extracted, are oriented so that they are elongated in a direction parallel to the axial direction. Therefore, we can assume that the grains were uniformly oriented inside the gauge region of the tensile specimens. Higher magnification optical micrographs from the center of each specimen show that the grains in the uncompressed specimen (see Figure 20c) had an average thickness of ~50 µm transverse to the axial direction (AD) while the compressed specimen (see Figure 20d) had an average thickness of ~52 µm. These data demonstrate that cryo-compression up to 30% strain was unable to produce a nano-crystalline material. This follows with the literature, where compressive strains of approximately 80% were necessary to achieve recrystallization. Such strains can be achieved via sheet/plate rolling (FT was able to achieve thickness reduction strains of up to 75% during rolling trials, see Table 2) but exceed PNNL's current cryo-compression capabilities.

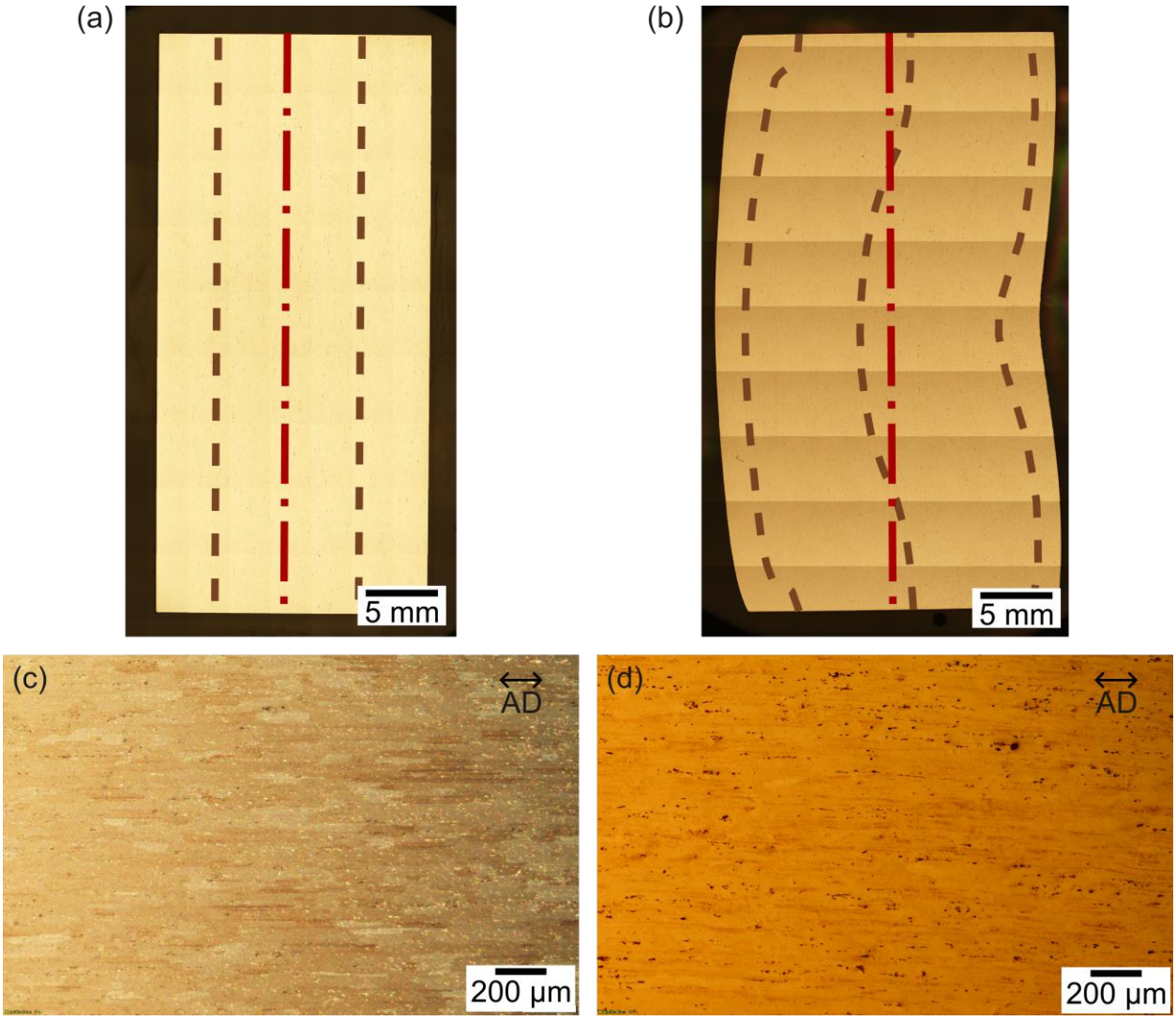

Fig. 20 Optical micrographs, captured with a polarized light filter, of 7075-T6 rod material. Stitched optical micrographs depict the cross-sectional area of (a) an uncompressed cylindrical specimen and (b) a specimen cryo-compressed to 30% strain. Red dot-dashed lines indicate the axis of each specimen, along which the rod was extruded and compressive strain was applied. Brown dashed lines indicate the direction along which grains were elongated. Higher magnification optical micrographs taken from the center of (c) the uncompressed cylindrical specimen and (d) the cryo-compressed specimen show grains that are elongated along the axial direction (AD) of their respective specimens. Source: PNNL

Conclusions

To support the development of a novel cryo stretch forming process, PNNL studied 7075 aluminum alloy material from rolling trials conducted by FT and conducted cryo-compression experiments. Under the experimental conditions employed, tensile strength exceeding the conventional T6 strength and a nanocrystalline microstructure was not achieved. The characterization and experimental work suggests that additional cryo-deformation strains are likely needed to achieve the target 700 MPa yield strength. The main results are summarized below.

1. Rod material that was cryo-compressed in liquid nitrogen (-196 °C) and at strain rates relevant for rolling processes could be compressed up to 60%. The maximum flow stress observed was 1150 MPa.

2. Cryo-compression increased the hardness of the W temper and accelerated both natural aging and artificial aging in 7075. Cryo-compression reduced the natural aging time required for hardness to stabilize from 91 hours to 24 hours. Cryo-compression also halved the time needed to reach 95% of the T6 hardness during artificial aging from 6 hours to 2.7 hours. These shortened aging times are attributed to the high dislocation density introduced during cryo-compression that accelerates the kinetics of η and η' precipitation.

3. Cryo-compression followed by a standard T6 heat treatment of 120 °C for 24 hours did not increase the hardness or strength of 7075 rod material. In fact, the slight decrease in yield strength and ultimate tensile strength (3% and 2% compared to the uncompressed material) with increasing amounts of cryo-compression suggests that the material may have been slightly overaged. This overaging after 24 hours T6 treatment is in line with the hardness evolution studies that suggest cryo-compression accelerates aging.

4. Cryo-compression to 30% compressive strain followed by a standard T6 heat treatment of 120 °C for 24 hours was unable to produce a nano-crystalline material. Greater compressive strain, such as the 75% thickness reduction strain achieved during FT's rolling trials, are likely needed to achieve recrystallization and produce a nano-crystalline microstructure.

5. While cryo-compression prior to a standard T6 heat treatment did not change the potentiodynamic behavior of 7075, it did make the open circuit potential slightly more positive and closer to that of the T73 temper, which is known for better stress-corrosion-cracking resistance compared to the peak-aged T6 temper. A more positive open circuit potential suggests that cryo-compression prior to artificial aging makes the material less amenable to corrosion. Further exploration is necessary to determine the significance of these results.

Subject Invention

None

Publications and Presentations

None

References

1. Zhao, Y. H., Liao, X. Z., Cheng, S., & Zhu, Y. T. (2006). Simultaneously Increasing the Ductility and Strength of Nanostructured Alloys. Advanced Materials, 18(17), 2280-2283.

2. Ovid'ko, I. A., Valiev, R. Z., & Zhu, Y. T. (2018). Review on superior strength and enhanced ductility of metallic nanomaterials. Progress in Material Science, 94, 462-540.

3. Lee, W. S., & Lin, C. R. (2016). Deformation behavior and microstructural evolution of 7075-T6 aluminum alloy at cryogenic temperatures. *Cryogenics*, *79*, 26-34.

Pacific Northwest National Laboratory

902 Battelle Boulevard
P.O. Box 999
Richland, WA 99354
1-888-375-PNNL (7665)

www.pnnl.gov